Optics & Laser Technology 135 (2021) 106700

Contents lists available at ScienceDirect

Optics and Laser Technology

journal homepage: www.elsevier.com/locate/optlastec

Full length article

Spectral approach to recognize spherical particles among non-spherical ones by angle-resolved light scattering

Ekaterina S. Yastrebova [a,b,c], Ivan Dolgikh [a,c], Konstantin V. Gilev [a,c], Irina V. Vakhrusheva [a,b], Elizaveta Liz [a,c], Alena L. Litvinenko [a,c], Vyacheslav M. Nekrasov [a,c], Dmitry I. Strokotov [a,d], Andrei A. Karpenko [b], Valeri P. Maltsev [a,c,*]

[a] Voevodsky Institute of Chemical Kinetics and Combustion SB RAS, 3 Institutskaya Str., Novosibirsk 630090, Russia
[b] Meshalkin National Medical Research Center, 15 Rechkunovskaya Str., 630055 Novosibirsk, Russia
[c] Novosibirsk State University, 2 Pirogova Str., Novosibirsk 630090, Russia
[d] Novosibirsk State Medical University, 52 Krasny Prospect, 630091 Novosibirsk, Russia

ARTICLE INFO

Keywords:
Flow cytometry
Light scattering
Blood cells
Optical particle sizing
Inverse problem

ABSTRACT

Most of known light-scattering technologies, which allow one to separate spherical from non-spherical single particles, utilize either analysis of 2D light-scattering pattern or depolarization of light scattered. Both approaches force one to use high-sensitive detectors to provide a suitable signal to noise ratio for two-dimensionless photo matrix or for optical system with crossed polarizers. In this study, we introduce the method for discrimination of spherical and non-spherical single particles. The approach is based on measurement of leading, most intensive, element S_{11} of light-scattering matrix. To provide maximal signal to noise ratio we specified the light-scattering profile (LSP) in terms of integrated over azimuthal angle S_{11} as a function of polar scattering angle. The shape-sensitive vector-invariant for individual spherical particles was constructed from the parameters of LSP spectrum. The vector-invariant plays a role of the numerical criterion to identify spherical particles from LSPs. It can be applied to find a sphere with characteristics ranging from 16.5 to 70 and from 0.5 to 7.0 for size and phase-shift parameters respectively (size parameter $\alpha = \pi d n_0/\lambda$, where d – sphere diameter, λ – wavelength of the incident light, and n_0 – medium refractive index, RI, phase-shift parameter $\rho = 2\alpha(m - 1)$, where relative RI $m = n/n_0$ and n is the sphere RI). These ranges cover all possible characteristics of blood cells within the visible region of wavelengths. The ability of the vector-invariant to recognize spherical cells among non-spherical ones was tested theoretically by LSP databases of optical models of platelets and mature red blood cells. Moreover, experimentally the vector-invariant demonstrated good performance in searching of near-perfect spheres among milk fat globules, isolated nuclei of mononuclear cells, and completely spherized cells in a course of red blood cell lysis.

1. Introduction

Discrimination between spherical and non-spherical single particles can play an important role in different environmental monitoring, biotechnological processes, and quality controls in production of powders. Light scattering may be attributed to the most valuable phenomenon which is used in such discrimination. Scientifically a perfect sphere gives an opportunity for precise experimental verification of adequate theoretical description of interaction between a physical field and the particle. In relation to the light scattering, a sphere is the simplest optical model of a particle that completely characterized by a size and refractive index (RI) only. These characteristics can be precisely retrieved from a solution of the inverse light-scattering (ILS) problem. Subsequently the RI of the substance forming the sphere will be useful in a study of optical properties of non-spherical particles consisting of the same substance.

Discrimination of spherical and non-spherical particles is especially important in biological cells. Determination of morphology of red blood cells (RBCs), platelets and lymphocyte nucleus could reveal a bulk of diseases and physiological states including raw of anemias, spherocytosis, cardiovascular and autoimmune disease, hemostasis and immune disorders [1–3]. Milk production quality control includes measurements of spheroidal milk fat globules (MFG) sizes and RI [4].

* Corresponding author at: Voevodsky Institute of Chemical Kinetics and Combustion SB RAS, Institutskaya 3, Novosibirsk 630090, Russia.
E-mail address: maltsev@kinetics.nsc.ru (V.P. Maltsev).

https://doi.org/10.1016/j.optlastec.2020.106700
Received 18 June 2020; Received in revised form 5 October 2020; Accepted 20 October 2020

Because of knotty shape and internal structure and high variability of morphological characteristics solution of ILS problem is highly complicated. Therefore determination of spherical particles among sample open a path to determine particle characteristics relatively simply by solution of ILS problem for spheres.

A spherical homogeneous particle illuminated by circularly polarized light will result in a pattern of scattered light, which is radially symmetrical about the axis of the illuminating beam. It means that asymmetry in scattering intensity as a function of an azimuthal angle with a fixed polar angle specifies an asphericity of particle analyzed. The analysis of the spatial intensity distribution of light scattered by a single particle may be a basis of methods to discriminate or classify particles. This phenomenon was widely exploited in instrumental solutions to identify spherical and non-spherical scatterers in particular with single particle aerosol analyzers [5].

Sachweb *et al* applied the DAWN-A single particle optical detector [6] to distinguish spherical and non-spherical airborne particles using a few photomultiplier tubes placed in different polar and azimuthal angles [7]. Hirst and Kaye utilized the aerofocusing transducer to deliver a particle into testing zone and the ellipsoidal reflector to construct the 2D light-scattering pattern on the high-sensitive intensified camera. The instrument examined both spherical and non-spherical particle types and appropriate theoretical comparisons were made with the experimental profiles using either Mie theory or a simple treatment based on the Rayleigh-Gans formalism. Both experimental and theoretical scattering data showed the good agreement for all particle types examined [8]. Definitely, an air as the surrounding medium in these experiments provided a sufficient amount of scattered photons even for 4-μm water droplets with the relative RI of 1.33. The substitution of air by water drops down an amount of photons scattered by a blood cell crucially. Nevertheless, the modern optics and electronics are able to provide sufficient signal to noise ratio for 2D imaging of biological cells in physiological solution [9]. The diffraction imaging cytometer acquires 2D light-scattering patterns from single cells within the angular interval of approximately ±18° for solid angle by a commercial CCD camera. The cytometer successfully demonstrated classification of different types of cells having a size of 5 μm or large with complex heterogeneity [10]. A few classifiers were applied in analysis of diffraction images to provide a reliable method to distinguish biological cells [11].

Depolarization of light scattered by a single particle could be also exploited in particle discriminators. Spherical particles do not change the state of polarization, whereas non-spherical particles cause the depolarization of the scattered light. Moreover, depolarization is very sensitive to variations of internal structure of biological cells. In particular, the depolarized orthogonal light scattering of conventional flow cytometers allows distinguishing eosinophils from neutrophils for direct clinical application. This phenomenon was experimentally discovered [12] and theoretically confirmed [13]. Parasitized red blood cells were successfully identified by a common flow cytometer enhanced by extra side-scattering detector with polarizer. In this particular case, the depolarization became the basis of reagent-free, real-time detection of drug effects [14]. Distinguishing between spherical and non-spherical airborne particles was realized by measure of the cross polarized scattered light by single particles into the near forward direction [15].

According to our long-term experience in the study of light scattering from blood cells with the original technology – scanning flow cytometry we have also tried to develop a discriminator for different types of cells. We utilized the common ways to construct a new approach. Firstly, we suggested and theoretically described the scanning flow cytometer (SFC) that allows the measurement of 2D light-scattering pattern of single particles [16].

Secondly, we demonstrated an ability of the modernized SFC to distinguish spherical and non-spherical single particles from analysis of polarizing properties of scattered light [17]. Unfortunately, these both approaches assume to modify the basic optical setup of the SFC that results to less stable operation of the instrument because of additional optical elements must be properly aligned and controlled during experiments. Extra challenge is caused by high sensitivity of depolarization and 2D scattering patterns to the optical alignment and the spatial calibration of the detectors. On the other hand, the high precision in solution of ILS problem for spheres realized by the SFC, may give exact quantitative data relating to blood cell compounds, in particular, optical constants for hemoglobin and the degree of homogeneity for cellular vesicles and nuclei.

These facts forced us to develop a method that allows discrimination of spherical and non-spherical individual particles by means of the simplest version of an optical setup in angle-resolved light scattering – unpolarized light in incidence and detection, integration over azimuth angle. Following to the Mueller matrix formalism it means that new method should allow us to recognize spherical particles among non-spherical ones just from measurement of leading element S_{11} of scattering matrix as a function of polar scattering angle θ with integration over azimuth angle φ, light-scattering profile (LSP). In this study, we introduce the numerical criterion, **optical vector-invariant**, for recognition of spherical particles that has been constructed from the spectral decomposition of the LSP.

2. Materials and methods

2.1. Red blood cells

After a written informed consent, blood was collected from a healthy volunteer by venipuncture into a vacuum tube containing ethylenediaminetetraacetic acid (EDTA) as anticoagulant. The sample was 1000-fold diluted in 0.9% saline and measured with the SFC. Hemolysis of the RBCs were performed according to the protocol described by Chernyshova et al [18]. The blood was placed into a lysing solution of ammonium chloride (0.15 M) to spherize RBCs.

Polystyrene microspheres of 4 μm (manufacturer specification) in mean size (Molecular Probes, USA) were added into all samples for SFC initialization (procedure described in details in [19]). All measurements were performed at room temperature (22 °C).

2.2. Isolated nuclei of mononuclear cells

Peripheral blood was collected from volunteers by venipuncture and placed into polystyrene tubes containing the potassium salt of EDTA as an anticoagulant. We transferred 3 ml of the blood into a 15 ml centrifuge tube and diluted it with an equal volume of PBS. We layered 6 ml of the diluted blood over 3 ml Lympholyte®-H (Cedarlane, CL5020) and centrifuged for 20 min at 800g at room temperature. After centrifugation, we carefully removed the cells from the interface containing peripheral blood mononuclear cells and transferred into a new centrifuge tube. We diluted the transferred cells with PBS to reduce the density of the solution and centrifuged at 800g for 10 min. The supernatant was discarded and the cells were washed in PBS by centrifugation at 450g for 10 min.

2.3. Milk fat globules

Raw whole bovine milk was obtained from a local individual farmer (Novosibirsk, Russian Federation) and was kept at 4 °C for up to 6 h before analysis. All samples were warmed to approximately 22 °C prior to measurement and diluted 50,000 times with distilled water. Approximately 10 thousand LSPs of milk fat globules (MFGs) were measured with the SFC.

2.4. Flow cytometer

The SFC can be attributed at the next generation of flow cytometers, since any analysis assigned for the ordinary flow cytometer can be carried out by means of the SFC. The main advantage of the SFC relates

to the measurement of the LSPs of individual cells contrary to the forward and side light scattering amplitudes measured by a common flow cytometer. An analysis of the LSP enhances the identification and characterization of single cells substantially. The SFC was fabricated by Cytonova LLC (Novosibirsk, Russia). The actual SFC was equipped by a 40 mW laser of 660 nm (LM-660-20-S) for illumination of individual cells and measurement of LSPs. The 488-nm laser (15 mW laser, FCD488-020, JDS Uniphase Corporation, Milpitas, California) was used to trigger the electronic unit of the SFC and to produce forward and side scattering signals in a conventional manner. The scheme of the optical system of the SFC is shown in Fig. 1. The mirror on the plate (PM) directs the focused beams into the optical cell (OC) for illumination of a particle. The spherical mirror of the OC reflects LSP (red cylinder in Fig. 1) to the PMTs. Detailed technical features of the SFC and the operational function of the optical cell were previously described elsewhere [17,20]. The operational angular range θ of the SFC was determined from the analysis of polystyrene microspheres [21] and was in range from 10° to 70°.

2.5. Theoretical methods

In the current study to solve direct and inverse light-scattering problems we utilized the following methods:

(1) Mie theory for simulation of the light scattered by a sphere by means of LabView codes developed on the basis of Bohren and Huffman program [22];
(2) Discrete Dipole approximation for simulation of light scattered by non-spherical particles, i.e. oblate spheroids, optical models of red blood cells, using the open-codes of the ADDA algorithm [23];
(3) DIRECT algorithm in solution of the ILS problem for spheres [24,25];

3. Theory/calculation

3.1. Definition of the optical vector-invariant

In our previous studies of spectral features of angle-resolved light scattering [26–30] we observed that a LSP spectrum is distorted when there are deviations in a shape or homogeneity of the sphere particle. Taking into account this fact, we formed the optical vector-invariant using two components: (1) the amplitude of non-zero peak of the LSP spectrum normalized at the zero-peak amplitude and (2) integral over the low-frequency wing of the non-zero peak of the spectrum in the following form:

$$I_{0.03} = \frac{1}{A_p}\int_{(L_p-0.03)}^{L_p} P(q)dq; \quad (1)$$

where $P(q)$ is the LSP amplitude spectrum, q is the spectral variable expressed in degrees^{-1}, L_p is the non-zero peak location, and A_p is the amplitude of the non-zero peak. The choice of the vector-invariant components was caused by our experience in the analysis of the RBC lysis kinetics with the SFC [31] where we already utilized the non-zero peak amplitude of the LSP spectrum to recognize spheres appeared in the end of the lysis. The second component of the vector-invariant has to

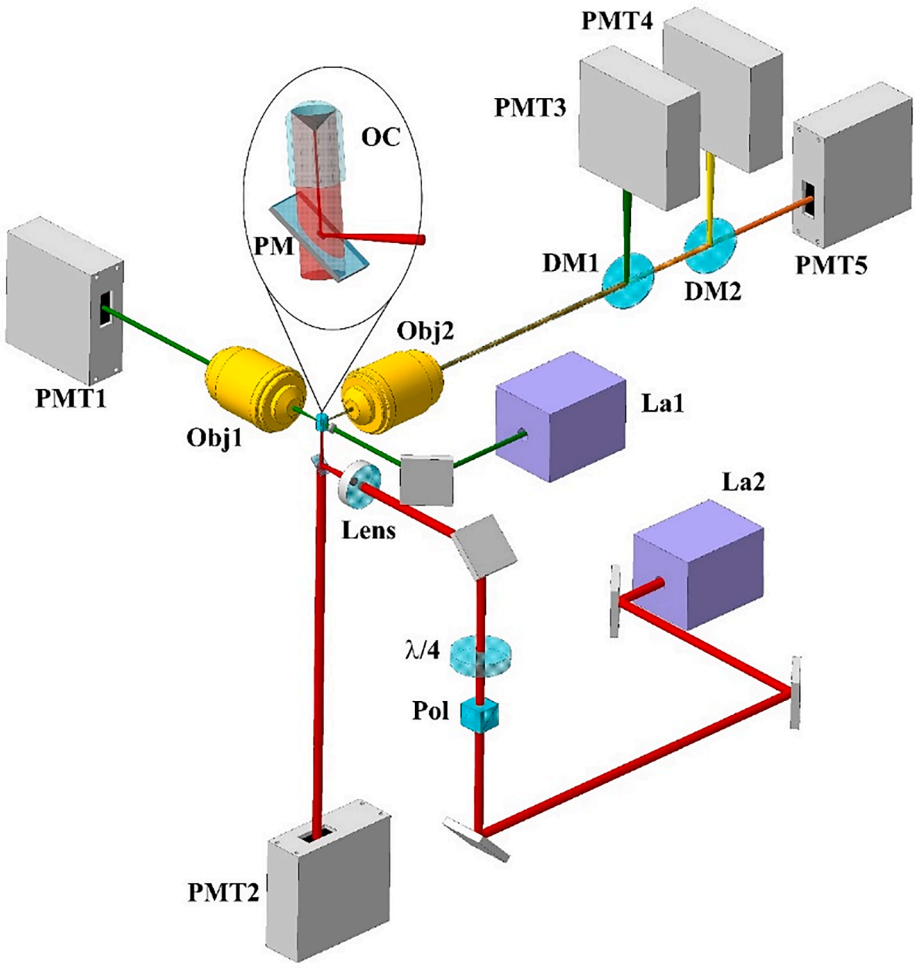

Fig. 1. The optical setup of the scanning flow cytometer exploited in the current experiments. PMT1-5, photomultiplier tubes: forward scatter, 660 nm light-scattering profile, side scatter, "yellow" fluorescence, "red" fluorescence, respectively; La1,2: 488 nm laser, 660 nm laser, respectively; DM1,2: dichroic mirrors; Obj1,2: objectives; Pol: polarizer; λ/4: quarter-wave plate; OC: optical cell; PM: plate with mirror. (For interpretation of the references to color in this figure legend, the reader is referred to the web version of this article.)

narrow the area where sphere can be recognized. We have found that the low-frequency wing of the non-zero peak becomes broader when a particle loses sphericity. Thereby, we defined the integral over the normalized non-zero peak within the interval of $0.03^{\circ -1}$ as the second component of the vector-invariant. The example that demonstrates the invariant construction is shown in Fig. 2. The LSP of the sphere with the size of 7 μm and RI of 1.37 was weighted by the LSP apparatus function described by Strokotov et al [25] (see Fig. 2A). Hereinafter the laser wavelength of 0.66 μm and medium RI of 1.333 were used in light-scattering simulation. Then we applied Blackman-Nuttall window with consequence Fourier transformation to get the LSP amplitude spectrum. The spectrum was normalized at zero-peak amplitude (Fig. 2B). The vector-invariant of $INV=\{0.433,\ 0.0215\}$ relates to the exemplified particle.

To define the applicable region for the vector-invariant $INV=\{A_p, I_{0.03}\}$ for spherical particles we calculated the LSPs for spheres using Mie theory for scattering angle range $\theta \in [10^{\circ}, 70^{\circ}]$. The sphere characteristics were varied within the ranges of size parameter $\alpha \in [16.5, 70]$ and phase-shift parameter $\rho \in [0.5, 7]$, where $\alpha = \pi d n_0/\lambda$ (d – sphere diameter, λ – wavelength of the incident light, and n_0 – medium RI), $\rho = 2\alpha(m-1)$, relative RI $m = n/n_0$ and n is the sphere RI. The corresponding particle RI versus size region is presented in Fig. 2C (black polygon).

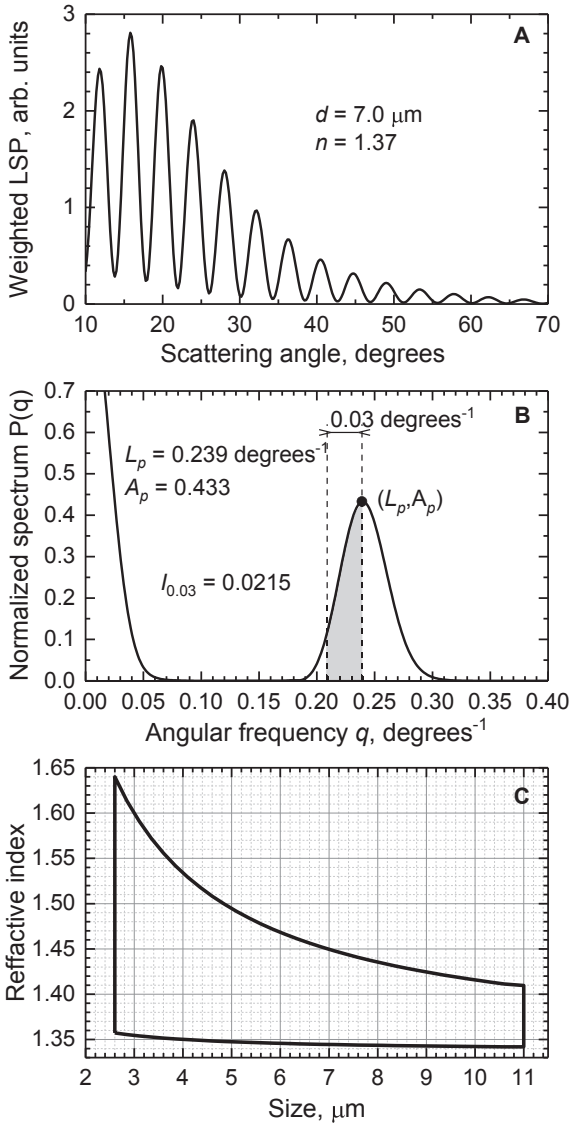

Fig. 2. The graph illustration for definition of the optical vector-invariant of a spherical particle: (A) weighted light-scattering profile (LSP) of a sphere with the characteristics shown; (B) windowed normalized Fourier amplitude spectrum of the LSP shown in (A). The vector-invariant $INV=\{A_p, I_{0.03}\}$ where A_p marked by point and $I_{0.03}$ is the integral over the area shown in gray color. (C) The area on the refractive index versus size map marked by black polygon defines characteristics of spheres that can be recognized by means of the optical vector-invariant.

4. Result and discussion

4.1. Optical vector-invariant: theoretical verification

We calculated the *INV* for the spheres with characteristics introduced in the Section 3.1 and constructed the $I_{0.03}$ versus A_p, map. These spheres have rather stable *INV*s forming the sphere region on the map. This

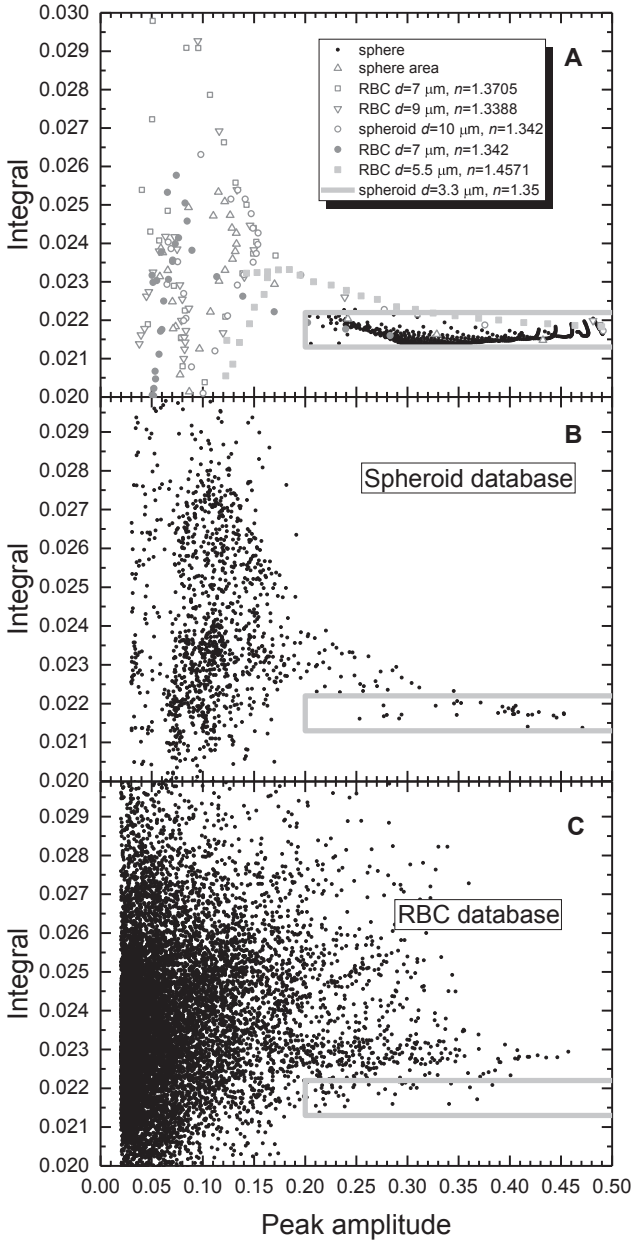

Fig. 3. The integral $I_{0.03}$ versus peak amplitude A_p maps. The rectangles marked in gray color border the area of spheres. (A) The rectangle involves all spheres (black circles) of interest. Differently shaped points show spheroids and non-spherical red blood cells (RBCs). (B) Six thousand seven hundred spheroids from the LSP database. (C) Fifteen thousand RBCs from the LSP database.

region is shown in Fig. 3A where each black point corresponds to the fixed sphere. Considering this region as the direct theoretical result that does not take into account an experimental noise, we have defined the sphere-rectangle formed by the values ranging from 0.2 to 0.5 and from 0.0213 to 0.0221 for the peak amplitude A_p and integral $I_{0.03}$, respectively. This sphere-rectangle is marked in gray color in Fig. 3. If a particle *INV* is not in the sphere-rectangle, we attribute this particle to non-spherical one. In order to understand where *INV*s of non-spherical particles are located on the map we calculated the LSPs of oblate spheroids and RBC models varying the sphericity index (*SI*) from 0.97 to 1.0. The *SI* is the ratio of the particle volume to the volume of sphere having the same surface area [32]. The volume, surface area and RI of the particles were kept unaltered in the simulation. The *INV*s of these particles are shown in Fig. 3A by differently shaped points. The particle characteristics presented in the box relate to spheres ($SI = 1$) with the diameter and RI indicated. According to this simulation all particles with the $SI < 0.998$ give the *INV* located outside the sphere-rectangle. This result demonstrates applicability of the *INV* in recognition near-perfect spheres from a LSP spectrum.

Additionally we tested the sphere-select ability of the *INV* on LSP databases of oblate spheroids and mature RBC models. We applied the same databases to solve the ILS problem for blood platelets and RBCs respectively [33,34]. The LSPs from databases were processed by calculating the *INV* from the LSP spectra. The *INV* maps for spheroids and RBCs are shown in Fig. 3B and C, respectively. There are only 0.5% of oblate spheroids inside of the sphere-rectangle with the $SI < 0.99$. The major part (0.2%) of the RBC models with $SI \geq 0.97$ falls into the sphere-rectangle. Indeed shapes of these particles are near to spherical: for RBC thickness and waist thickness almost equal to diameter and spheroid aspect ratio tends to 1. Considering the simulation introduced in Fig. 3 we would like to emphasize the role of the second component of the vector-invariant in the precise recognition of spheres. Previously used recognizing algorithm attributed a particle to non-spherical one if the peak amplitude A_p exceeded 0.2. The current version of the algorithm allowed us to attribute the rather big amount of spheroids and RBC models to non-spherical particles. The results presented in Fig. 3 demonstrate this fact indeed.

4.2. Recognition of sphered RBC during hemolysis

The reason of this study was caused by the appearance of LSP spectra with amplitudes of the non-zero peaks higher than 0.2 at the end of RBC hemolysis experiment. In a course of lysis a RBC shape is transformed from biconcave to sphere due to a change of osmolarity by ammonium chloride. The theory of RBC lysis developed by Chernyshev et al. [31] allows one to simulate RBC *SI* as a function of time and to estimate the transforming duration of RBC shape. A LSP of a particle is rather sensitive to the particle shape and dependency of the LSP on the particle shape can be observed in spectral domain. In particular the mean amplitude of the maximal non-zero peaks in the LSP spectra is increased during the lysis. Typical dependency of the peak amplitudes on the lysing time is shown in Fig. 4A where one point corresponds to a single RBC. The cells with high peak amplitudes appear in approximately 6 min after hemolysis initiation. The *INV* map of the same cells is shown in Fig. 4B. It demonstrates the localization of the major part of the high amplitude cells inside of the sphere-rectangle. Therefore, we were easily able to recognize the RBCs, which were spherized during the lysis. This performance of the new approach in recognition of spheres is crucial for detail characterization of cells and cellular components with the SFC.

One more arresting note is that one can easily observe in Fig. 4A and B the “gap” in the peak amplitudes between non-spherical and spherized RBCs. In order to clarify the reason of the “gap” appearance we calculated the LSPs using RBC models. All RBC characteristics kept unaltered except the *SI*. The dependency of the peak amplitudes as a function of *SI* is shown in Fig. 4C. This dependency demonstrates the strong rise just before $SI = 1$. Assuming the constant rate of spherization we have to

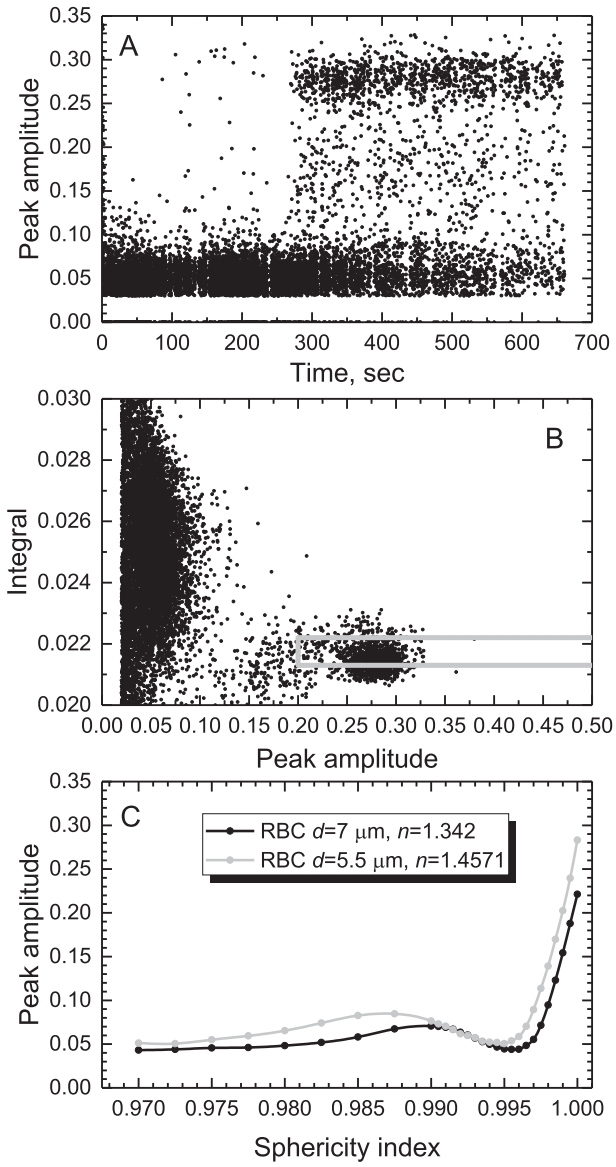

Fig. 4. RBC lysis. (A) the peak amplitude as a function of a time when a cell triggers the SFC trace recorder; (B) *INV* map of RBCs in hemolysis; (C) the peak amplitude as a function of sphericity index of RBC optical models. The RBC characteristics shown in the frame relate to the cells with $SI = 1$.

expect a small amount of RBCs with peak amplitude ranging from 0.1 to 0.2 that is in agreement with experimentally measured RBCs during the lysis.

4.2.1. Characterization of sphered RBCs

The usage of the *INV* has allowed us to identify the spherical RBCs among non-spherical ones. These spherical RBCs can be precisely characterized by means of solution of the ILS problem. We have processed all LSPs of RBCs which *INV*s are located inside of the sphere-rectangle, near-perfect sphere, and outside the sphere-rectangle but with the peak amplitude above 0.2, like-sphere (Fig. 4B). The solution gives us the size and RI of each RBC with its uncertainties. The results of the LSP processing are presented in Table 1. It includes parameters of distributions over RBC diameters, RIs and hemoglobin (Hb) contents are shown. Additionally we introduce the median errors for RBC characteristics which are retrieved from LSPs measured with SFC. Errors are obtained from the solution of the ILS problem using Mie theory.

To demonstrate the agreement between experimental and theoretical

Table 1
Parameters of distribution of two fractions of spherized RBCs. SD = standard deviation.

Parameter	Near-perfect spheres	Like-spheres
Fraction, counts	435	65
Mean diameter (SD), μm	5.90 (0.45)	5.51 (0.57)
Mean RI (SD)	1.3851 (0.0111)	1.3975 (0.0151)
Mean Hb content (SD), pg	26.3 (4.0)	26.6 (4.7)
Median error of diameter, nm	21	27
Median error of RI	0.0009	0.0015
Median error of Hb content, pg	0.6	0.7

LSPs we chose two LSPs from both RBC fractions, near-perfect sphere (Fig. 5A) and like-sphere (Fig. 5B). The chosen LSPs were fitted by the Mie theory to determine the size and RI of spherized RBCs. The results of the solution of the ILS problem are shown in the text boxes in Fig. 5. First, we would like to emphasize the high precision in analysis of spherized RBCs. The median error of RBC diameters is 21 nm and 27 nm for near-perfect sphere and like-sphere RBCs respectively. This resolution in size of particles exceeds in one order of magnitude the fundamental resolution of optical microscopy. High precision relates to the other characteristic of RBC such as refractive index that can be used in calculation of Hb content in an individual RBC. The Hb content and Hb concentration play the diagnosis role in hematological analysis and high precision in their determination improves the quality of analysis for patients. Have to note that we used the specific refraction increment 0.0019 dl/g in evaluation of Hb concentration from RI on the basis published studies [35,36]. Second, the precision in analysis of the near-perfect RBC spheres exceeds the analogues precision for the like-sphere RBCs that proves the performance of the vector-invariant *INV* in accurate recognition of spherical particles.

4.3. Recognition of spherical MFGs, homogeneous isolated nuclei of mononuclear cells and blood platelets

In order to demonstrate the applicability of the optical vector-invariant in recognition of spheres among other particles we analyzed the MFGs, isolated nuclei of mononuclear cells and blood platelets with the SFC. The measured LSPs were used in construction of the LSP spectra and *INV* calculation according to the algorithm introduced in Section 3.1. The results of recognition are presented in Fig. 6.

In particular, the Fig. 6A demonstrates the *INV* map for MFGs. In our previous analysis of MFGs with the SFC a few years ago [37] we found that a part of the MFGs is far from spheres. We applied the oblate spheroid as the MFG optical model to determine individual MFG characteristics: equi-volume diameter, aspect ratio, RI. In order to recognize spherical MFGs we utilized the F-test using the null hypothesis of spherical model with 5% significance level. To realize the F-test we solved the ILS problem two times for both sphere and spheroid models of the MFG. Currently we are able to calculate the *INV* from the measured LSPs and specify spherical MFG inside of the sphere-rectangle (Fig. 6A). According to this method, we have attributed approximately 11% of MFGs to near-perfect spheres. Taking into account the applicability region of the *INV* approach which is only for spheres with a diameter above 2.6 μm, the percentage of the sphere fraction in MFGs looks

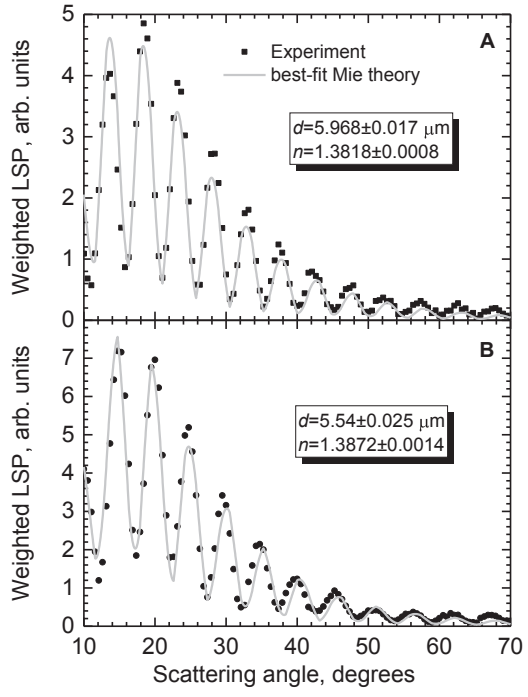

Fig. 5. Characterization of the spherized RBCs from the LSPs. A) the most often appeared near-perfect sphered RBC and B) the most often appeared like-sphere RBC.

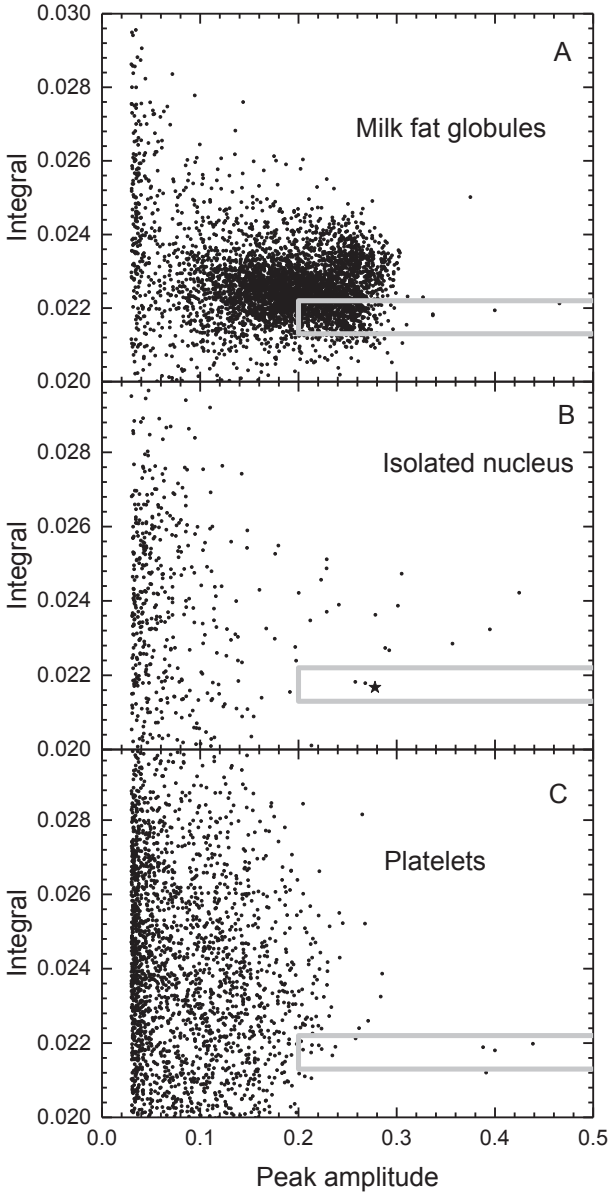

Fig. 6. The *INV* maps for (A) milk fat globules, (B) isolated nuclei of mononuclear cells and (C) platelets.

reasonable (see Fig. 4 in [37]).

The vector-invariant is sensitive to a particle inhomogeneity in analogous manner to its sphericity. The peak amplitude A_p, drops down when a sphere loses homogeneity. Theoretically we observed this effect in our study of optical properties of neutrophils [27]. In this work, we measured the LSPs of isolated nuclei of mononuclear cells with the SFC and constructed the *INV* map to recognize most homogeneous spheres among them. Our experimental and theoretical study of light scattering of the mononuclear cells allowed us to conclude that nucleus inhomogeneity resulted to substantial disagreement between experimental and calculated LSPs for the covered homogeneous sphere model [25]. The current experimental analysis of the isolated nuclei confirms this conclusion. There are less than 0.1% of nuclei in the sample with the *INV*s located inside the sphere-rectangle (Fig. 6B). We characterized the nuclei which *INV*s are located in the sphere-rectangle. The LSP of the nucleus (with *INV* marked by star in Fig. 6B) was used in the solution of the ILS problem. The characteristics of the nucleus shown in Fig. 7A.

The vector-invariant has allowed us to identify the near-perfect sphere platelets. There are 14 cells inside of the sphere-rectangle in the Fig. 6C. Totally we analyzed 22 thousands platelets in the sample that gives less than 0.1% for relative concentration of near-perfect sphere platelets. Indeed platelets attributed to the balloon phenotype are shaped close to a sphere [38]. Processing of the LSP of the platelet identified as a near-perfect sphere showed good agreement between experimentally measured LSP and LSP calculated from the Mie theory (Fig. 7B). The result of the solution of the ILS problem for this platelet is shown in the frame.

5. Conclusion

With this study, we have introduced the novel approach in recognition of individual spherical particles among non-spherical ones. This approach was realized in the simplest instrumental way. It is based on measuring the most intensive light-scattering profile, i.e. unpolarized and integrated over azimuthal angle, to provide the highest signal to noise ratio in analysis of individual particles from light scattering. Here, the use of combination of these two features (unpolarized and integrated light) in light-scattering registration leads to more accurate signals compare to other methods. Moreover, the high signal to noise ratio becomes indispensable in analysis of biological cells, which refractive index is very close to the refractive index of surrounded medium, usually saline buffer. We successfully utilized the high sensitivity of the novel numerical criterion in recognition of spherized RBCs during hemolysis in appropriate buffer.

One more useful essential feature of the novel sphere-recognizing engine allows us to identify of spherical particles in a real-time mode in the continuous way of a sample analysis. If sample contains differently shaped particles, the optical vector-invariant of spheres will be directly placed into the sphere-rectangle of the *INV* map. Recognized spherical particles can be immediately characterized from the solution of the ILS problem with parametrization [28] or best-fit to Mie theory. The modern personal computers are able to perform the fitting iterations with Mie theory in tens microseconds. Have to note that this method for characterization of single particles does not require any calibration of the SFC. It gives the nice opportunity for independent absolute comparison of cell characterization in different laboratories around the world. The laser wavelength plays a role of the scaling unit of particle sizing. However, the suggested approach can be utilized for particle size more than 2.6 μm in visible wavelength range. The applicable dimension limit is possible to overcome by usage of ultraviolet region. In current work such experiments is not presented because we predominantly applied method to blood cells analysis.

The best advantage of the SFC relates to characterization of an individual sphere with record precision. For instance, the size and RI of individual spheres were determined with errors of less than 10 nm and a few thousandth, respectively [19,20,29,39]. Relating to the spherized RBCs, the obtained high precision of the RI results in determination of hemoglobin content in individual RBCs with the record accuracy. In the current experiments the Hb content for the near-perfect sphere RBCs was measured with median precision of approximately 2% that is really best than ever before. We believe that high precision on measurement of hemoglobin contents in individual RBCs will allow us to determine the oxy-/deoxy-hemoglobin ratio from analysis of two LSPs measured at two wavelength simultaneously for each particle. This ratio could be included at the 48 diagnosis RBC indices that can be measured by means of SFC.

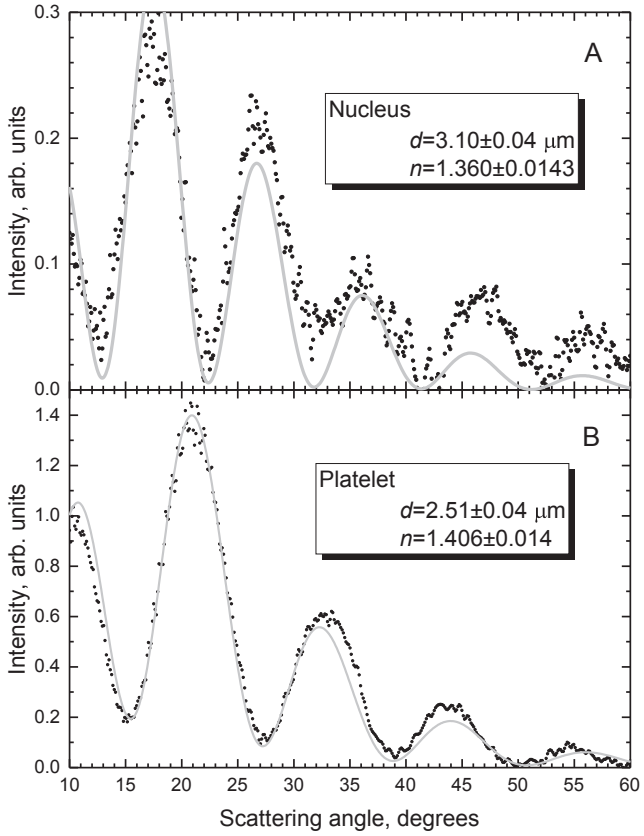

Fig. 7. The weighted light-scattering profiles (experiment – points, best-fit theory – line) of the isolated nucleus and platelet. Result of characterization of the cells in size and RI presented in the frames.

CRediT authorship contribution statement

Ekaterina S. Yastrebova: Investigation, Writing - review & editing. **Ivan Dolgikh:** Formal analysis. **Konstantin Gilev:** Software. **Irina Vakhrusheva:** Investigation. **Elizaveta Liz:** Investigation, Resources. **Alena L. Litvinenko:** Investigation, Visualization. **Vyacheslav Nekrasov:** Data curation, Formal analysis. **Dmitry I. Strokotov:** Investigation. **Andrei A. Karpenko:** Resources, Funding acquisition. **Valeri P. Maltsev:** Conceptualization, Methodology, Writing - review & editing, Supervision.

Declaration of Competing Interest

The authors declare that they have no known competing financial interests or personal relationships that could have appeared to influence the work reported in this paper.

Acknowledgements

This work was supported by the Russian Science Foundation (grant

No. 18-75-10030).

References

[1] M. Diez-Silva, M. Dao, J. Han, C.-T. Lim, S. Suresh, Shape and biomechanical characteristics of human red blood cells in health and disease, MRS Bull. 35 (5) (2010) 382–388, https://doi.org/10.1557/mrs2010.571.

[2] C. BRIGGS, Quality counts: new parameters in blood cell counting, Int. J. Lab. Hematol. 31 (3) (2009) 277–297, https://doi.org/10.1111/j.1751-553X.2009.01160.x.

[3] A.J. Gale, Continuing education course #2: current understanding of hemostasis, Toxicol. Pathol. 39 (1) (2011) 273–280, https://doi.org/10.1177/0192623310389474.

[4] C. Lopez, Milk fat globules enveloped by their biological membrane: Unique colloidal assemblies with a specific composition and structure, Curr. Opin. Colloid Interface Sci. 16 (5) (2011) 391–404, https://doi.org/10.1016/j.cocis.2011.05.007.

[5] P.H. Kaye, Spatial light-scattering analysis as a means of characterizing and classifying non-spherical particles, Meas. Sci. Technol. 9 (2) (1998) 141–149, https://doi.org/10.1088/0957-0233/9/2/002.

[6] P.J. Wyatt, K.L. Schehrer, S.D. Phillips, C. Jackson, Y.-J. Chang, R.G. Parker, D. T. Phillips, J.R. Bottiger, Aerosol particle analyzer, Appl. Opt. 27 (2) (1988) 217, https://doi.org/10.1364/AO.27.000217.

[7] B.A. Sachweh, W.D. Dick, P.H. McMurry, Distinguishing between spherical and nonspherical particles by measuring the variability in azimuthal light scattering, Aerosol. Sci. Technol. 23 (3) (1995) 373–391, https://doi.org/10.1080/02786829508965321.

[8] E. Hirst, P.H. Kaye, Experimental and theoretical light scattering profiles from spherical and nonspherical particles, J. Geophys. Res. 101 (D14) (1996) 19231–19235, https://doi.org/10.1029/95JD02343.

[9] K.M. Jacobs, J.Q. Lu, X.-H. Hu, Development of a diffraction imaging flow cytometer, Opt. Lett. 34 (19) (2009) 2985, https://doi.org/10.1364/OL.34.002985.

[10] J. Zhang, Y. Feng, M.S. Moran, J.Q. Lu, L.V. Yang, Y.u. Sa, N. Zhang, L. Dong, X.-H. Hu, Analysis of cellular objects through diffraction images acquired by flow cytometry, Opt. Express 21 (21) (2013) 24819, https://doi.org/10.1364/OE.21.024819.

[11] W. Wang, Y. Wen, J.Q. Lu, L. Zhao, S.A. Al-Qaysi, X.-H. Hu, Rapid classification of micron-sized particles of sphere, cylinders and ellipsoids by diffraction image parameters combined with scattered light intensity, J. Quant. Spectrosc. Radiat. Transfer 224 (2019) 453–459, https://doi.org/10.1016/j.jqsrt.2018.12.010.

[12] B.G. de Grooth, L.W.M.M. Terstappen, G.J. Pupples, J. Greve, Light-scattering polarization measurements as a new parameter in flow cytometry, Cytometry 8 (6) (1987) 539–544, https://doi.org/10.1002/cyto.990080602.

[13] M.A. Yurkin, K.A. Semyanov, V.P. Maltsev, A.G. Hoekstra, Discrimination of granulocyte subtypes from light scattering: theoretical analysis using a granulated sphere model, Opt. Express 15 (25) (2007) 16561, https://doi.org/10.1364/OE.15.016561.

[14] M. Rebelo, C. Sousa, H.M. Shapiro, M.M. Mota, M.P. Grobusch, T. Hänscheid, S. Borrmann, A novel flow cytometric hemozoin detection assay for real-time sensitivity testing of plasmodium falciparum, PLoS ONE 8 (4) (2013) e61606, https://doi.org/10.1371/journal.pone.0061606.s003.

[15] T. Clauss, A. Kiselev, S. Hartmann, S. Augustin, S. Pfeifer, D. Niedermeier, H. Wex, F. Stratmann, Application of linear polarized light for the discrimination of frozen and liquid droplets in ice nucleation experiments, Atmos. Meas. Tech. 6 (4) (2013) 1041–1052, https://doi.org/10.5194/amt-6-1041-2013.

[16] G.V. Dyatlov, K.V. Gilev, K.A. Semyanov, V.P. Maltsev, The scanning flow cytometer modified for measurement of two-dimensional light-scattering pattern of individual particles, Meas. Sci. Technol. 19 (1) (2008) 015408, https://doi.org/10.1088/0957-0233/19/1/015408.

[17] D.I. Strokotov, A.E. Moskalensky, V.M. Nekrasov, V.P. Maltsev, Polarized light-scattering profile-advanced characterization of nonspherical particles with scanning flow cytometry: polarized light scattering, Cytometry 79A (7) (2011) 570–579, https://doi.org/10.1002/cyto.a.21074.

[18] E.S. Chernyshova, Y.S. Zaikina, G.A. Tsvetovskaya, D.I. Strokotov, M.A. Yurkin, E. S. Serebrennikova, L. Volkov, V.P. Maltsev, A.V. Chernyshev, Influence of magnesium sulfate on HCO 3 /Cl transmembrane exchange rate in human erythrocytes, J. Theor. Biol. 393 (2016) 194–202, https://doi.org/10.1016/j.jtbi.2015.12.023.

[19] J.T. Soini, A.V. Chernyshev, P.E. Hanninen, E. Soini, V.P. Maltsev, A new design of the flow cuvette and optical set-up for the scanning flow cytometer, Cytometry 31 (2) (1998) 78–84, https://doi.org/10.1002/(SICI)1097-0320(19980201)31:2<78::AID-CYTO2>3.0.CO;2-E.

[20] V.P. Maltsev, Scanning flow cytometry for individual particle analysis, Rev. Sci. Instrum. 71 (1) (2000) 243–255, https://doi.org/10.1063/1.1150190.

[21] A.I. Konokhova, M.A. Yurkin, A.E. Moskalensky, A.V. Chernyshev, G. A. Tsvetovskaya, E.D. Chikova, V.P. Maltsev, Light-scattering flow cytometry for identification and characterization of blood microparticles, J. Biomed. Opt. 17 (5) (2012) 057006, https://doi.org/10.1117/1.JBO.17.5.057006.

[22] C.F. Bohren, D.R. Huffman, Absorption and Scattering of Light by Small Particles, Wiley, 1983.

[23] M.A. Yurkin, A.G. Hoekstra, The discrete-dipole-approximation code ADDA: Capabilities and known limitations, J. Quant. Spectrosc. Radiat. Transfer 112 (13) (2011) 2234–2247, https://doi.org/10.1016/j.jqsrt.2011.01.031.

[24] D.R. Jones, C.D. Perttunen, B.E. Stuckman, Lipschitzian optimization without the Lipschitz constant, J. Optim. Theory Appl. 79 (1) (1993) 157–181, https://doi.org/10.1007/BF00941892.

[25] D.I. Strokotov, M.A. Yurkin, K.V. Gilev, D.R. van Bockstaele, A.G. Hoekstra, N. B. Rubtsov, V.P. Maltsev, Is there a difference between T- and B-lymphocyte morphology? J. Biomed. Opt. 14 (6) (2009) 064036, https://doi.org/10.1117/1.3275471.

[26] K.A. Semyanov, P.A. Tarasov, A.E. Zharinov, A.V. Chernyshev, A.G. Hoekstra, V. P. Maltsev, Single-particle sizing from light scattering by spectral decomposition, Appl. Opt. 43 (26) (2004) 5110, https://doi.org/10.1364/AO.43.005110.

[27] D.Y. Orlova, M.A. Yurkin, A.G. Hoekstra, V.P. Maltsev, Light scattering by neutrophils: model, simulation, and experiment, J. Biomed. Opt. 13 (5) (2008) 054057, https://doi.org/10.1117/1.2992140.

[28] A.V. Romanov, A.I. Konokhova, E.S. Yastrebova, K.V. Gilev, D.I. Strokotov, A. V. Chernyshev, V.P. Maltsev, M.A. Yurkin, Spectral solution of the inverse Mie problem, J. Quant. Spectrosc. Radiat. Transfer 200 (2017) 280–294, https://doi.org/10.1016/j.jqsrt.2017.04.034.

[29] A.I. Konokhova, E.S. Yastrebova, D.I. Strokotov, A.V. Chernyshev, A.A. Karpenko, V.P. Maltsev, Ultimate peculiarity in angular spectrum enhances the parametric solution of the inverse Mie problem, J. Quant. Spectrosc. Radiat. Transfer 235 (2019) 204–208, https://doi.org/10.1016/j.jqsrt.2019.06.034.

[30] A.V. Romanov, A.I. Konokhova, E.S. Yastrebova, K.V. Gilev, D.I. Strokotov, V. P. Maltsev, M.A. Yurkin, Sensitive detection and estimation of particle non-sphericity from the complex Fourier spectrum of its light-scattering profile, J. Quant. Spectrosc. Radiat. Transfer 235 (2019) 317–331, https://doi.org/10.1016/j.jqsrt.2019.07.001.

[31] A.V. Chernyshev, P.A. Tarasov, K.A. Semianov, V.M. Nekrasov, A.G. Hoekstra, V. P. Maltsev, Erythrocyte lysis in isotonic solution of ammonium chloride: theoretical modeling and experimental verification, J. Theor. Biol. 251 (1) (2008) 93–107, https://doi.org/10.1016/j.jtbi.2007.10.016.

[32] K.V. Gilev, M.A. Yurkin, E.S. Chernyshova, D.I. Strokotov, A.V. Chernyshev, V. P. Maltsev, Mature red blood cells: from optical model to inverse light-scattering problem, Biomed. Opt. Express 7 (4) (2016) 1305, https://doi.org/10.1364/BOE.7.001305.d001.

[33] A.E. Moskalensky, M.A. Yurkin, A.I. Konokhova, D.I. Strokotov, V.M. Nekrasov, A. V. Chernyshev, G.A. Tsvetovskaya, E.D. Chikova, V.P. Maltsev, Accurate measurement of volume and shape of resting and activated blood platelets from light scattering, J. Biomed. Opt. 18 (1) (2013) 017001, https://doi.org/10.1117/1.JBO.18.1.017001.

[34] K.V. Gilev, E.S. Yastrebova, D.I. Strokotov, M.A. Yurkin, N.A. Karmadonova, A. V. Chernyshev, V.V. Lomivorotov, V.P. Maltsev, Advanced consumable-free morphological analysis of intact red blood cells by a compact scanning flow cytometer, Cytometry 91 (2017) 867–873, https://doi.org/10.1002/cyto.a.23141.

[35] J.L. Stoddard, G.S. Adair, The refractometric determination of hemoglobin, J. Biol. Chem. 57 (1923) 437–454.

[36] H. Zhao, P. Brown, P. Schuck, On the distribution of protein refractive index increments, Biophys. J. 100 (9) (2011) 2309–2317, https://doi.org/10.1016/j.bpj.2011.03.004.

[37] A.I. Konokhova, A.A. Rodionov, K.V. Gilev, I.M. Mikhaelis, D.I. Strokotov, A. E. Moskalensky, M.A. Yurkin, A.V. Chernyshev, V.P. Maltsev, Enhanced characterisation of milk fat globules by their size, shape and refractive index with scanning flow cytometry, Int. Dairy J. 39 (2) (2014) 316–323, https://doi.org/10.1016/j.idairyj.2014.08.006.

[38] J.W.M. Heemskerk, W.M.J. Vuist, M.A.H. Feijge, C.P.M. Reutelingsperger, T. Lindhout, Collagen but not fibrinogen surfaces induce bleb formation, exposure of phosphatidylserine, and procoagulant activity of adherent platelets: evidence for regulation by protein tyrosine kinase-dependent Ca2+ responses, Blood 90 (7) (1997) 2615–2625, https://doi.org/10.1182/blood.V90.7.2615.

[39] A.I. Konokhova, D.N. Chernova, D.I. Strokotov, A.A. Karpenko, A.V. Chernyshev, V.P. Maltsev, M.A. Yurkin, Light-scattering gating and characterization of plasma microparticles, J. Biomed. Opt. 21 (11) (2016) 115003, https://doi.org/10.1117/1.JBO.21.11.115003.